

**Supporting Information
for
Adsorption, Dissociation and Dehydrogenation of Water
Monomer and Water Dimer on the Smallest 3D
Aluminum Particle. The O-H Dissociation Barrier
Disappears for the Dimer**

Jerzy Moc*

Faculty of Chemistry, Wroclaw University, F. Joliot-Curie 14, 50-383 Wroclaw, Poland

Corresponding Author: Tel. (48)(71) 375-7267

*E-mail: jerzy.moc@chem.uni.wroc.pl

Contents:

1. Full references 33, 41.
2. (a) Singlet octahedral **R1** ($D_{3d}^1 A_{1g}$), (b) Triplet prism **R2** ($D_{3h}^3 A_1'$), (c) Singlet prism **R3** ($C_{2v}^1 A_1$) structures of Al_6 , and singlet (d) **P1** ($C_{2v}^1 A_1$), (e) **P2** ($C_s^1 A'$), (f) **P3** ($C_s^1 A'$) structures of Al_6O , and (g) Transition state **TSP1-3** ($C_s^1 A'$) for interconversion between the **P1** and **P3** isomers of Al_6O (with the corresponding imaginary frequency) (Figure S1).
3. CCSD(T)/aug-cc-pVTZ energy profile for the $\text{Al}_6 + \text{H}_2\text{O} \rightarrow \text{Al}_6\text{O} + \text{H}_2$ reaction calculated at the B3LYP/aug-cc-pVTZ geometries, with (zero-point energy) ZPE (B3LYP) corrections (Figure S2).
4. B3LYP/aug-cc-pVTZ energy profile for the $\text{Al}_6 + \text{H}_2\text{O} \rightarrow \text{Al}_6\text{O} + \text{H}_2$ reaction calculated at the B3LYP/aug-cc-pVTZ geometries, with (zero-point energy) ZPE (B3LYP) corrections (Figure S3).
5. **P1d** and **P2d** isomers of the $\text{H}_2\text{O}-\text{Al}_6\text{O}$ product of the reaction of the water dimer with Al_6 optimized at the B3LYP/aug-cc-pVTZ level (Figure S4).
6. B3LYP/aug-cc-pVTZ energy profile for the $\text{Al}_6 + (\text{H}_2\text{O})_2 \rightarrow \text{H}_2\text{O}-\text{Al}_6\text{O} + \text{H}_2$ reaction calculated at the B3LYP/aug-cc-pVTZ geometries, with (zero-point energy) ZPE (B3LYP) corrections (Figure S5).
7. CCSD(T)/aug-cc-pVTZ energy profile for the $\text{Al}_6 + (\text{H}_2\text{O})_2 \rightarrow \text{H}_2\text{O}-\text{Al}_6\text{O} + \text{H}_2$ reaction calculated at the B3LYP/aug-cc-pVTZ geometries, with (zero-point energy) ZPE (B3LYP) corrections (Figure S6).
8. Imaginary mode of the transition state **TS3d-4d** of the path 1dim (Figure S7).

Full reference 33.

Gaussian 09: Frisch, M. J.; Trucks, G. W.; Schlegel, H. B.; Scuseria, G. E.; Robb, M. A.; Cheeseman, J. R.; Scalmani, G.; Barone, V.; Mennucci, B.; Petersson, G. A.; Nakatsuji, H.; Caricato, M.; Li, X.; Hratchian, H. P.; Izmaylov, A. F.; Bloino, J.; Zheng, G.; Sonnenberg, J. L.; Hada, M.; Ehara, M.; Toyota, K.; Fukuda, R.; Hasegawa, J.; Ishida, M.; Nakajima, T.; Honda, Y.; Kitao, O.; Nakai, H.; Vreven, T.; Montgomery, Jr., J. A.; Peralta, J. E.; Ogliaro, F.; Bearpark, M.; Heyd, J. J.; Brothers, E.; Kudin, K. N.; Staroverov, V. N.; Kobayashi, R.; Normand, J.; Raghavachari, K.; Rendell, A.; Burant, J. C.; Iyengar, S. S.; Tomasi, J.; Cossi, M.; Rega, N.; Millam, N. J.; Klene, M.; Knox, J. E.; Cross, J. B.; Bakken, V.; Adamo, C.; Jaramillo, J.; Gomperts, R.; Stratmann, R. E.; Yazyev, O.; Austin, A. J.; Cammi, R.; Pomelli, C.; Ochterski, J. W.; Martin, R. L.; Morokuma, K.; Zakrzewski, V. G.; Voth, G. A.; Salvador, P.; Dannenberg, J. J.; Dapprich, S.; Daniels, A. D.; Farkas, Ö.; Foresman, J. B.; Ortiz, J. V.; Cioslowski, J.; Fox, D. J. *Gaussian 09, Revision C.01*, Gaussian, Inc., Wallingford CT, 2009.

Full reference 41.

MOLPRO: Werner, H.-J.; Knowles, P. J.; Knizia, G.; Manby, F. R.; Schütz, M.; Celani, P.; Korona, T.; Lindh, R.; Mitrushenkov, A.; Rauhut, G.; Shamasundar, K. R.; Adler, T. B.; Amos, R. D.; Bernhardsson, A.; Berning, A.; Cooper, D. L.; Deegan, M. J. O.; Dobbyn, A. J.; Eckert, F.; Goll, E.; Hampel, C.; Hesselmann, A.; Hetzer, G.; Hrenar, T.; Jansen, G.; Köppl, C.; Liu, Y.; Lloyd, A. W.; Mata, R. A.; May, A. J.; McNicholas, S. J.; Meyer, W.; Mura, M. E.; Nicklass, A.; O'Neill, D. P.; Palmieri, P.; Peng, D.; Pflüger, K.; Pitzer, R.; Reiher, M.; Shiozaki, T.; Stoll, H.; Stone, A. J.; Tarroni, R.; Thorsteinsson, T.; Wang, M. *MOLPRO*, version 2012.1; Cardiff University: Cardiff, U.K., 2012.

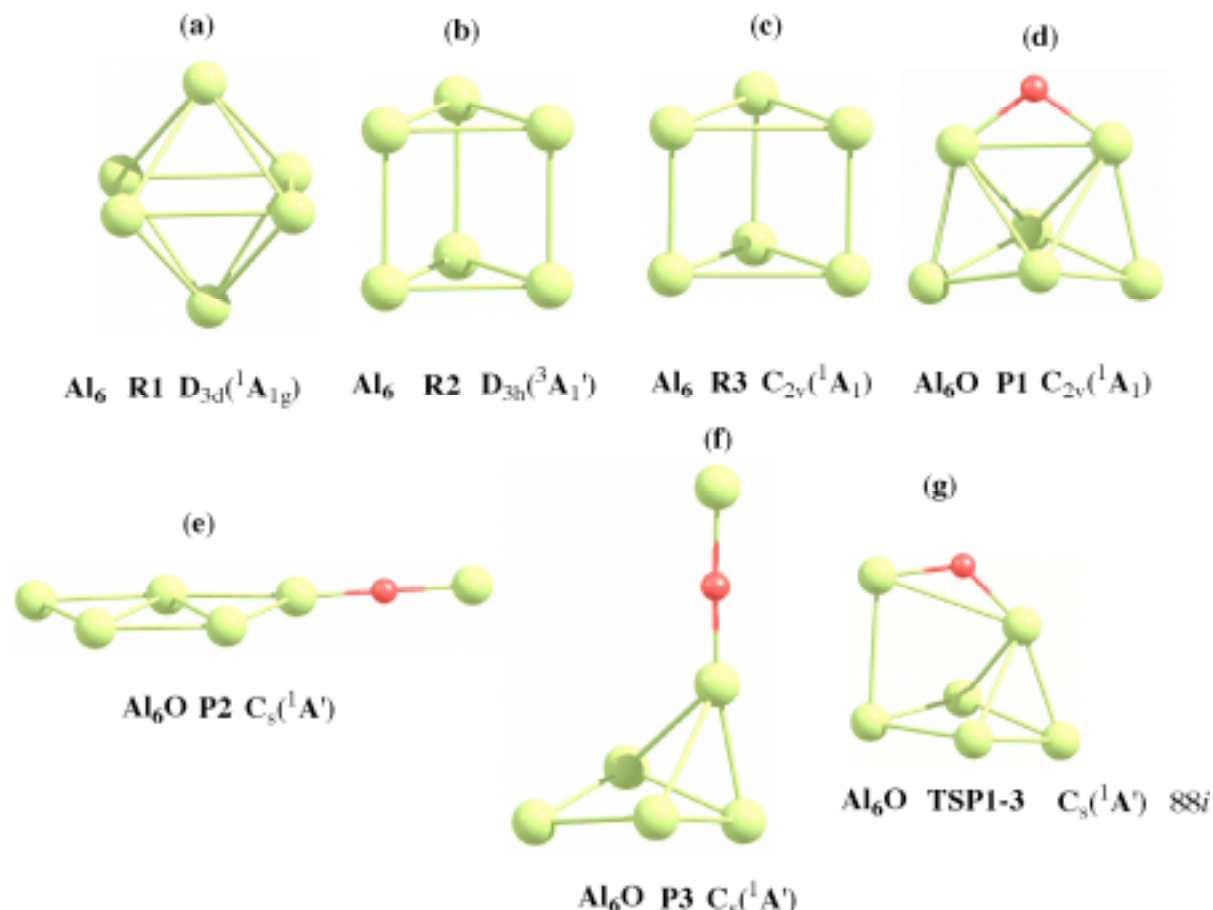


Figure S1.

Caption to Figure S1. (a) Singlet octahedral **R1** ($D_{3d}^1 A_{1g}$), (b) Triplet prism **R2** ($D_{3h}^3 A_1'$), (c) Singlet prism **R3** ($C_{2v}^1 A_1$) structures of Al_6 , and singlet (d) **P1** ($C_{2v}^1 A_1$), (e) **P2** ($C_s^1 A'$), (f) **P3** ($C_s^1 A'$) structures of Al_6O , and (g) Transition state **TSP1-3** ($C_s^1 A'$) for interconversion between the **P1** and **P3** isomers of Al_6O (with the corresponding imaginary frequency) (Figure S1). All structures are optimized at the B3LYP/aug-cc-pVTZ level.

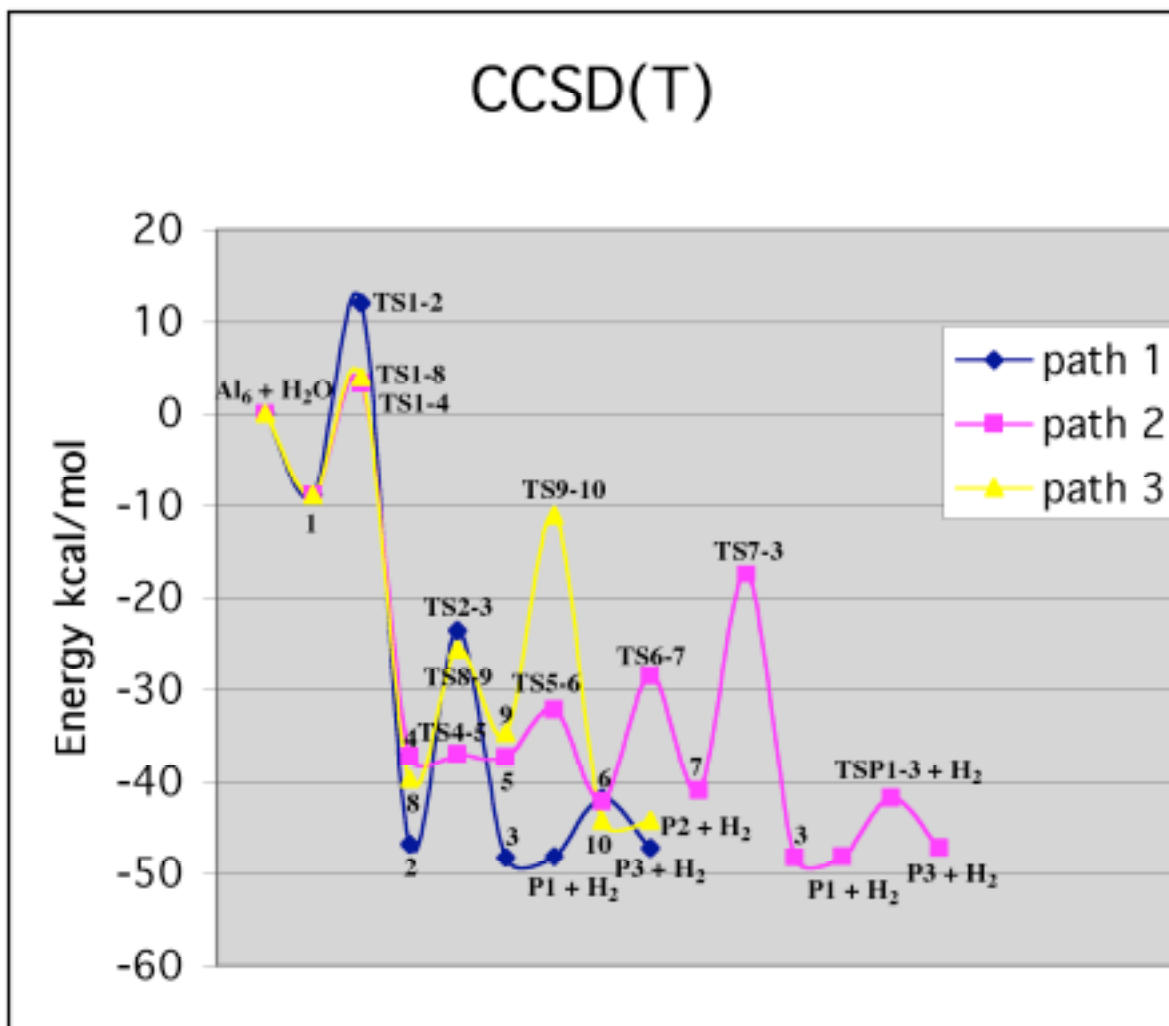
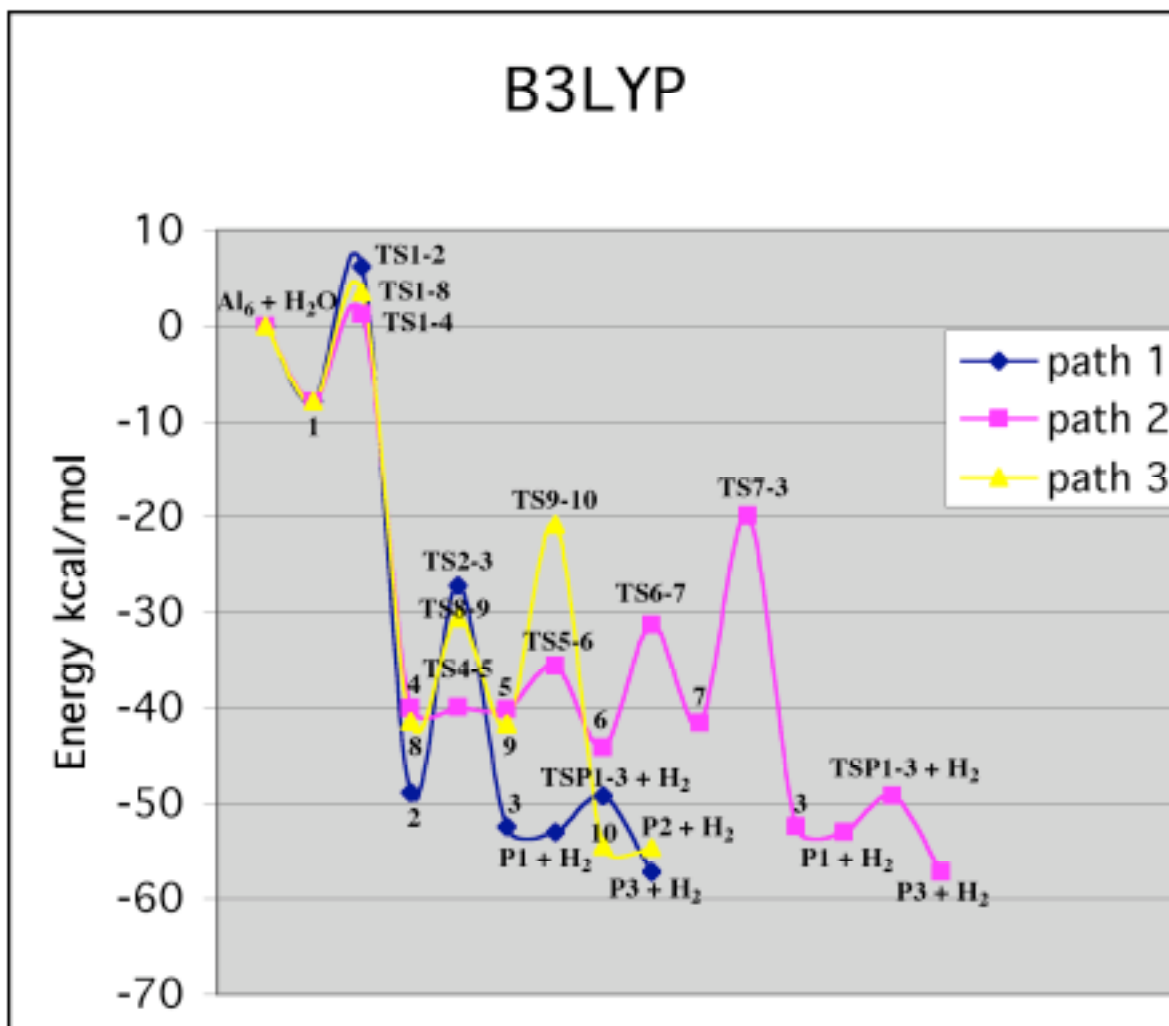


Figure S2.

Caption to Figure S2. CCSD(T)/aug-cc-pVTZ energy profile for the $\text{Al}_6 + \text{H}_2\text{O} \rightarrow \text{Al}_6\text{O} + \text{H}_2$ reaction calculated at the B3LYP/aug-cc-pVTZ geometries, with (zero-point energy) ZPE (B3LYP) corrections.

**Figure S3.**

Caption to Figure S3. B3LYP/aug-cc-pVTZ energy profile for the $\text{Al}_6 + \text{H}_2\text{O} \rightarrow \text{Al}_6\text{O} + \text{H}_2$ reaction calculated at the B3LYP/aug-cc-pVTZ geometries, with (zero-point energy) ZPE (B3LYP) corrections.

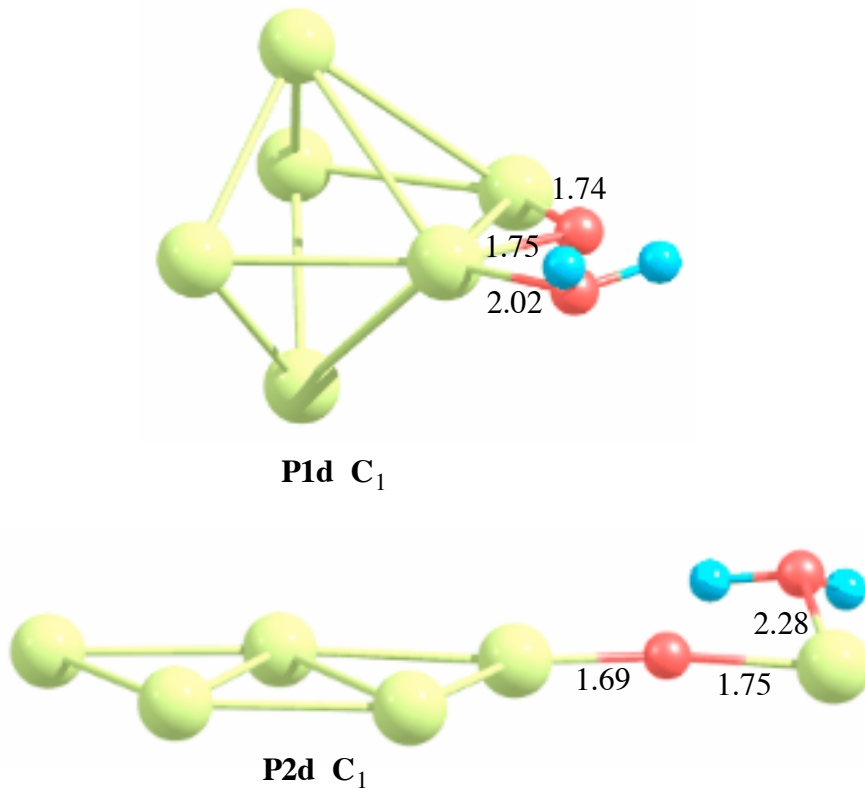


Figure S4.

Caption to Figure S4. **P1d** and **P2d** structures of the H₂O-Al₆O product of the reaction of the water dimer with Al₆ optimized at the B3LYP/aug-cc-pVTZ level.

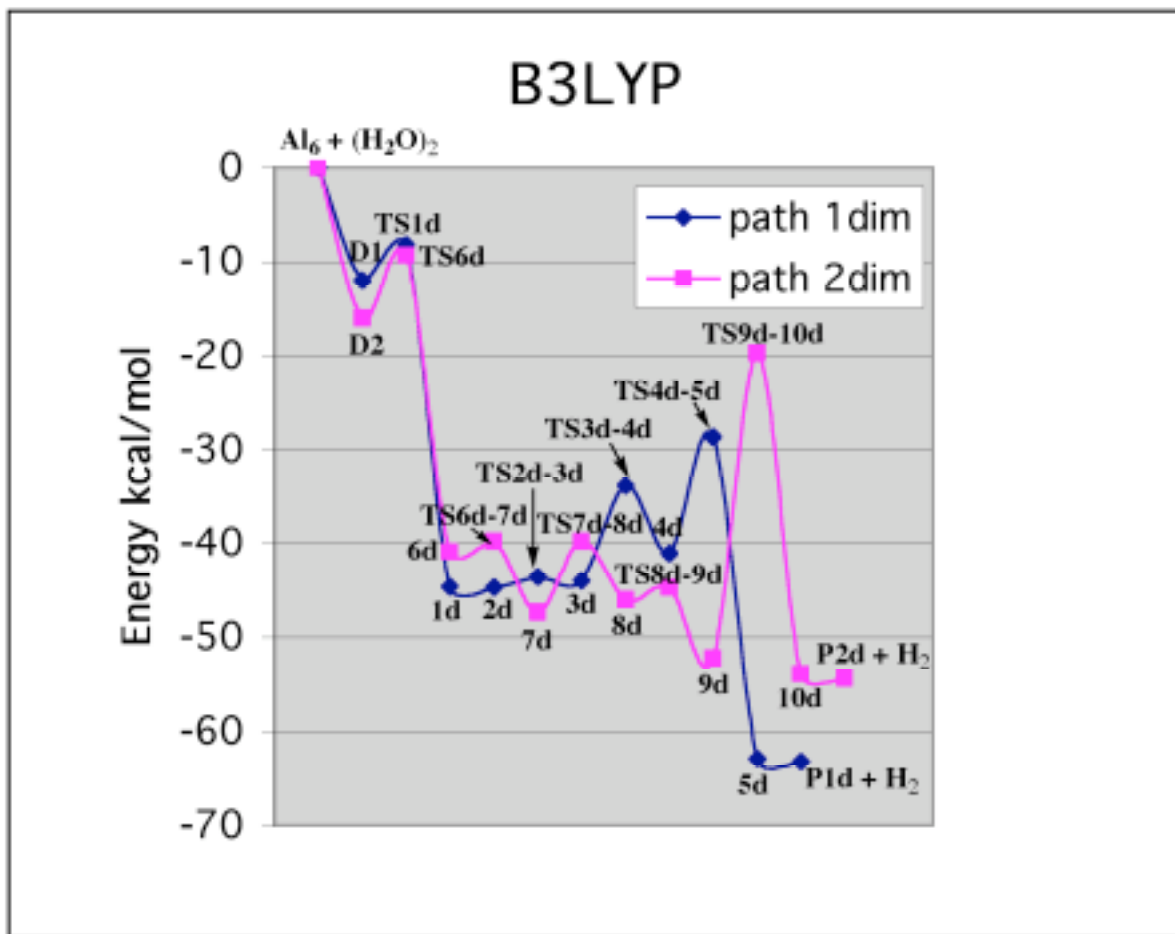


Figure S5.

Caption to Figure S5. B3LYP/aug-cc-pVTZ energy profile for the $\text{Al}_6 + (\text{H}_2\text{O})_2 \rightarrow \text{H}_2\text{O}-\text{Al}_6\text{O} + \text{H}_2$ reaction calculated at the B3LYP/aug-cc-pVTZ geometries, with (zero-point energy) ZPE (B3LYP) corrections.

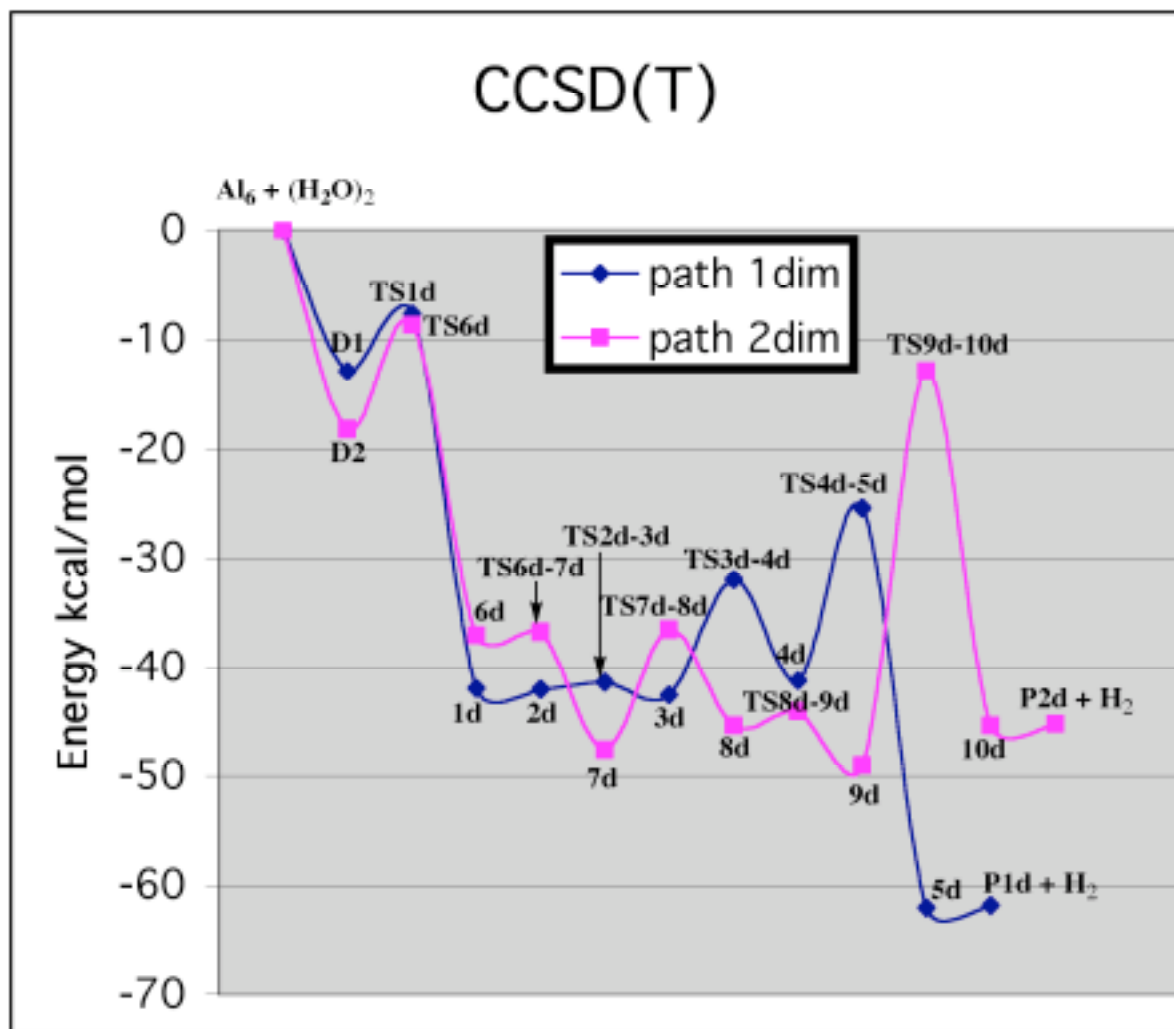


Figure S6.

Caption to Figure S6. CCSD(T)/aug-cc-pVTZ energy profile for the $\text{Al}_6 + (\text{H}_2\text{O})_2 \rightarrow \text{H}_2\text{O-Al}_6\text{O} + \text{H}_2$ reaction calculated at the B3LYP/aug-cc-pVTZ geometries, with (zero-point energy) ZPE (B3LYP) corrections.

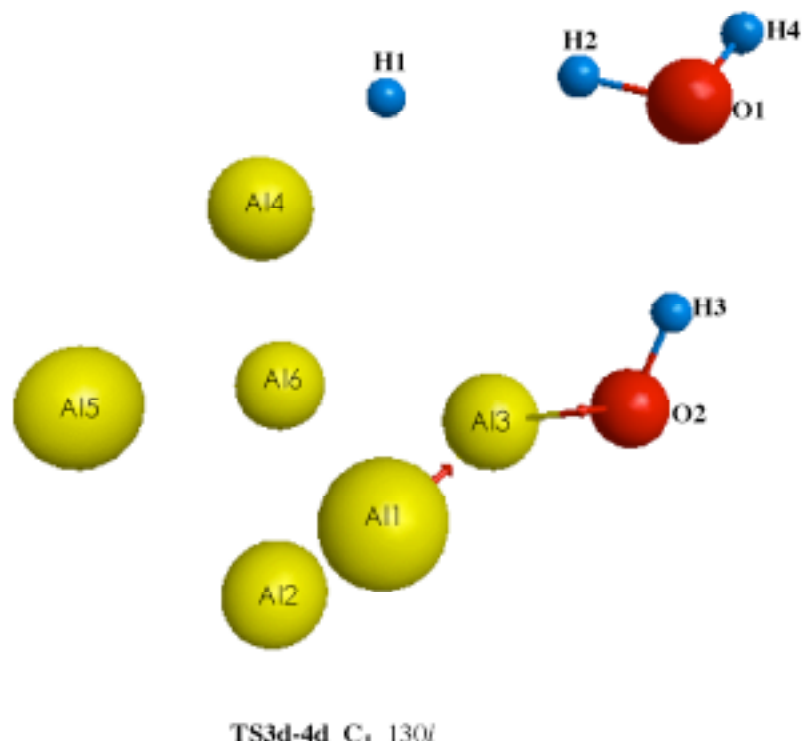


Figure S7.

Caption to Figure S7. Imaginary mode of the transition state **TS3d-4d** of the path 1dim.